

Final Draft

of the original manuscript

Carpenter, J.R.; Guha, A.:
Blocking effects on mean ocean currents by offshore wind farm foundations.
In: Physical Review Fluids. Vol. 9 (2024) 103802.

First published online by American Physical Society: 11.10.2024

https://dx.doi.org/10.1103/PhysRevFluids.9.103802

Blocking effects on mean ocean currents by offshore wind farm foundations

Jeffrey R. Carpenter*
Institute for Coastal Ocean Dynamics,
Helmholtz-Zentrum Hereon, Geesthacht 21502, Germany

Anirban Guha
School of Science and Engineering,
University of Dundee, Dundee, UK

(Dated: August 22, 2024)

Abstract

The continued development of shallow continental shelf regions with offshore wind farm (OWF) structures raises the question of what potential hydrodynamic impacts may be expected. One such impact is a reduction in the ocean currents that results from the additional frictional drag from the turbine foundation structures. To understand this potential 'blocking' effect, we construct a fluid mechanical model consisting of an idealised circular patch of OWF with increased friction. The idealised OWF is then subjected to a steady mean flow superimposed on much stronger elliptical tidal currents – a common scenario in shelf seas with OWF installations. Due to the quadratic dependence of friction on fluid velocity, the elliptical tidal currents result in a linearised friction acting on the mean flow that is no longer parallel to the mean flow. This 'anisotropic' friction has the effect of deflecting, in addition to reducing, the mean flow in the region of the OWF. However, it is found that a good approximation to the reduction of flow caused by OWFs can be obtained by the simplest linear, isotropic representation of the friction, i.e., a linear drag law. The flow reduction within the OWFs is found to be primarily dependent on the ratio of the increase in drag coefficient inside the farm to that of the surroundings, with weaker dependencies on the parameters describing the tidal ellipse. The magnitudes of the flow reductions in the idealised model appear to be in approximate agreement with more realistic modelling results, and are expected to capture the basic balance of the mean flow in the blocking of ocean currents by many OWFs in the North Sea, especially with increasing size in future development scenarios.

I. INTRODUCTION

In efforts to shift energy production to more carbon neutral forms, there has been a rapid expansion of offshore wind farm (OWF) development in coastal waters [1, 2]. To reach promised levels of sustainable energy production, many governments are currently planning rapid expansions of OWF resources in the near future [3]. There is therefore a pressing need to understand and quantify any potential impacts of these offshore developments on the physical oceanography of coastal seas [4–6]. These potential physical changes are expected to have cascading effects that may have the potential to alter marine productivity [7, 8] and higher trophic levels, such as fish and whale populations [4, 9].

* jeff.carpenter@hereon.de

Changes in the physical oceanography arising from OWFs can be expected through the production of turbulent wakes in both the atmosphere [10–12] and ocean [13–15]. Although important contributions to ocean currents could arise from the altered wind stress on the ocean surface [12, 16], we neglect this aspect of the potential oceanographic changes to focus on the changes induced by the interaction of ocean currents with the OWF foundation structures. Such an interaction has been found to lead to turbulence levels that are increased from the natural environment [15, 17], which cause changes to the stratification [14–16, 18, 19], and to mean ocean currents [19]. Little effect is expected to tidal currents (see [20], and section VI).

This study is motivated by the finding in Christiansen et al.[19] that OWFs in the southern North Sea are capable of altering mean (i.e. non-tidal) currents by as much as 10% of existing values. We therefore, undertake an idealised theoretical study of this process in order to better understand the basic physics at work. The model that we employ has been first discussed in Garrett and Cummins[21], where they present an analytical study that approximates the 'blocking' effects of a circular region of structures with increased friction in a shallow shelf sea subject to tides. The goal of Garrett and Cummins [21] was to understand feedbacks between tidal energy extraction and tidal friction. Some of these solutions are outlined below in the context of understanding similar effects in offshore wind farms. Presently, we extend the Garrett and Cummins [21] study by allowing for a modified anisotropic friction term that results from the quadratic nature of the bottom friction in the presence of strong tidal currents. We therefore examine the blocking effects of *mean* currents (i.e. those resulting from averaging over many tidal cycles) by OWFs, while accounting for the dominant tidal currents and how they are capable of modifying the bottom friction.

The paper consists of a mathematical formulation of the problem, where we outline a basic derivation of the equations and boundary conditions that apply. We then find solutions for two special cases: (i) perfectly circular tidal currents which leads to a linear frictional drag formulation, and (ii) the limit of infinite friction within the OWF, where it can effectively be replaced by a circular impenetrable boundary. Then, we solve the full problem and relate it to the special cases above when examining the effects of variable tidal current parameters and OWF friction levels. Finally, we apply the idealised model findings to make predictions for three North Sea OWFs, and find similar blocking effects of the mean currents to the more realistic modelling study of Christiansen et al. [19] for two of the OWFs, and a negligible

impact on the currents for the other OWF.

II. PROBLEM FORMULATION

Our model of the circulation of mean currents in shallow shelf seas consists of the shallow water equations on an f-plane, subject to quadratic friction. Mathematically this is written as

$$\frac{\partial \vec{u}}{\partial t} + \vec{u} \cdot \vec{\nabla}\vec{u} + \vec{f} \times \vec{u} + g\vec{\nabla}h = -\frac{C_D}{H+h}|\vec{u}|\vec{u} \tag{1}$$

with $\vec{u} = (u, v, 0)$ the depth mean horizontal velocity on the horizontal Cartesian coordinate system $(x, y, 0)$, $\vec{f} = (0, 0, f)$ the vertical component of the Coriolis vector, g the gravitational acceleration, h the elevation of the sea surface with respect to the still water depth H, and C_D the frictional drag coefficient. We assume that variations in h are over a much larger scale than the region of interest. Then we can take the horizontal mean flow to be divergence free [21], so

$$\vec{\nabla} \cdot \vec{u} = 0. \tag{2}$$

This allows us to represent the flow by a stream function, ψ, such that $\vec{u} = (\partial\psi/\partial y, -\partial\psi/\partial x)$.

Furthermore, we will only look for steady solutions of the above equation with the non-linear term neglected. Justification for this approximation is considered later on.

A. Friction of offshore wind farms

In this study, the current alterations of offshore wind farms are accounted for through their modification of the drag coefficient, C_D, in (1). Drag forces per unit area arising from the boundary layer that develops over the sea bed are typically represented by the drag law

$$\vec{F} = -\rho_0 C_D^0 |\vec{u}|\vec{u}, \tag{3}$$

where we denote a representative water density by ρ_0, and the sea bed drag coefficient by C_D^0. The presence of the foundation structures give rise to an additional drag force on the currents, above that provided by the sea bed. We quantify this by the following drag law (see [14]) for the force per unit horizontal area

$$\vec{F} = -\frac{\rho_0 C_D^t A_f}{2\ell^2}|\vec{u}|\vec{u}, \tag{4}$$

with the structure specific drag coefficient given by C_D^t, the frontal area of the structure by A_f, and a typical horizontal spacing of the structures represented by the distance ℓ. Although the drag force of each structure will manifest itself as a turbulent wake, we concern ourselves with the mean overall effect of the entire farm (composed of many structures) once the various individual wakes have merged. Therefore, we increase the background (sea bed) drag coefficient, C_D^0, by the value $C_D^t A_f/(2\ell^2)$ within the OWF area to quantify the OWF effect. An important dimensionless parameter that is used to quantify this increase in friction is the friction ratio [21], $q \equiv C_D^t A_f/(2C_D^0\ell^2)$, giving the ratio between the additional structure-induced friction, and the background. Typical values of these parameters have been tabulated for a number of OWFs in the North Sea in Table I, and a discussion is presented in section V.

In our estimates of the friction ratio and drag coefficients we have neglected the effects of any scour protection measures that often take the form of an irregular rock layer around the structure base. This would be expected to lead to additional friction that is not accounted for.

B. Friction in strong tidal flows

The quadratic friction term makes analytical solutions difficult. However, it is possible to simplify this term by considering a flow that is composed of two components, $\vec{u} = \vec{u}_0 + \vec{u}_1$, where $\vec{u}_0$ represents the relatively small and (presumed) steady mean flow, and $\vec{u}_1$ the larger amplitude and rapidly varying tidal currents. We assume that $|\vec{u}_0| \ll |\vec{u}_1|$; a situation that is generally true in many coastal seas, where OWFs are constructed (see Table I for typical values). We note that the nonlinear frictional drag term can then be approximated through

$$\frac{C_D}{H}|\vec{u}|\vec{u} \approx \mathbf{K}\vec{u}_0 \equiv \begin{bmatrix} K_{xx} & K_{xy} \\ K_{yx} & K_{yy} \end{bmatrix} \vec{u}_0 \tag{5}$$

following [22]. This approximation is accurate to order $O(|\vec{u}_1|/|\vec{u}_0|)$. We now define $\mathbf{K} \equiv c\,\mathbf{k}$, where $c = C_D/H$ so we can write

$$\mathbf{k} = \begin{bmatrix} k_{xx} & k_{xy} \\ k_{yx} & k_{yy} \end{bmatrix} \tag{6}$$

TABLE I. Parameter estimates for OWF foundation geometries, tidal, and mean flow currents, at three wind farms in the North Sea: BARD 1 Offshore (54.4°N, 6.0°E), Global Tech (54.5°N, 6.4°E), and the Dogger Bank group consisting of Dogger Bank A,B,C and Sophia (55°N, 2.2°E).

		Wind Farm		
Parameter	Symbol (Unit)	BARD 1	Global Tech	Dogger Bank
Foundation geometry:				
Frontal area	A_f (m^2)	402	560	$155-300$
Turbine spacing	ℓ (m)	866	733	2450
Drag coefficient	C_D^t (-)	1.0	1.0	1.0
Depth	H (m)	40	40	$18-35$
M2 Tidal currents:				
Tidal amplitude	$\tilde{u}$ (m s^{-1})	0.41	0.41	0.26
Ellipse axis ratio	$\tilde{b}$ (-)	0.11	0.15	0.29
Orientation	$\tilde{\theta}$ (°)	-14	-23	6
Mean flow:				
Magnitude	U (m s^{-1})	0.026	0.020	0.022
Direction	λ_0 (°)	45	90	127
Dimensionless control parameters:				
Friction ratio	q (-)	0.11	0.21	≤ 0.01
Mean/tidal current ratio	$\lvert\vec{u}_0/\vec{u}_1\rvert$ (-)	0.06	0.05	0.08
Nonlinearity parameter	ξ (-)	$O(1)$	$O(1)$	$0.3-0.6$
Model predictions:				
Reduction	(-)	0.048	0.086	< 0.01
Deflection	(°)	< 1	< 1	< 1

where

$$k_{xx} = \left\langle \frac{2u_1^2 + v_1^2}{|\vec{u}_1|} \right\rangle, \quad k_{yy} = \left\langle \frac{u_1^2 + 2v_1^2}{|\vec{u}_1|} \right\rangle, \quad k_{xy} = k_{yx} = \left\langle \frac{u_1 v_1}{|\vec{u}_1|} \right\rangle \tag{7}$$

with the angled brackets referring to an average over a suitable period that is long compared to the dominant tidal periods.

In practise, we will represent the tidal currents by a single tidal frequency component that take the form of a tidal ellipse, and average over this tidal period. Mathematically, this

can be written

$$u_1(t) = \tilde{u}[\cos(\omega t)\cos(\tilde{\theta}) - \tilde{b}\sin(\omega t)\sin(\tilde{\theta})], \quad v_1(t) = \tilde{u}[\cos(\omega t)\sin(\tilde{\theta}) + \tilde{b}\sin(\omega t)\cos(\tilde{\theta})] \quad (8)$$

where $0 \leq \tilde{b} \leq 1$ is the ratio of the minor to major axes of the current ellipse. It represents how elliptic the currents are, with $\tilde{b} = 0$ giving rectilinear currents, and $\tilde{b} = 1$ circular currents. Note that taking $\tilde{b} < 0$ gives a change in the ellipse rotation direction, however, the $\mathbf{k}$ components are invariant to this change and we keep $\tilde{b} > 0$ without loss of generality. The orientation of the major axis of the ellipse is given by $\tilde{\theta}$. Using this form for the tidal currents means we can express the friction tensor components as $k_{ij} = \tilde{u} f(\tilde{b}, \tilde{\theta})$.

Using the tidal friction tensor form for the friction term, results in a single equation for ψ, which henceforth represents the streamfunction of the steady mean flow. The equation is derived by taking the vertical component of the curl of (1), using (5). This is expressed as $\hat{k} \cdot (\vec{\nabla} \times \mathbf{K}\vec{u}) = 0$, with $\hat{k}$ the vertical unit vector. In terms of ψ we can expand this to

$$L_1[\psi] + L_2[\psi] = 0 \quad (9)$$

where we have denoted

$$L_1 \equiv K_{yy}\frac{\partial^2}{\partial x^2} - 2K_{xy}\frac{\partial^2}{\partial x \partial y} + K_{xx}\frac{\partial^2}{\partial y^2}. \quad (10)$$

and

$$L_2 \equiv \Big(\frac{\partial K_{yy}}{\partial x} - \frac{\partial K_{xy}}{\partial y}\Big)\frac{\partial}{\partial x} + \Big(\frac{\partial K_{xx}}{\partial y} - \frac{\partial K_{xy}}{\partial x}\Big)\frac{\partial}{\partial y}. \quad (11)$$

C. OWF geometry

In order to facilitate the development of analytical solutions, we choose an idealised OWF geometry that is represented by a circular region of radius R, as in Garrett and Cummins [21]. The boundary of the OWF is denoted throughout by Γ. We then take the friction coefficient to have a constant background value, c_0, and an increase to $c_0 + c_t$ within the circular OWF. This can be written mathematically as

$$c(r) = c_0 + c_t\mathcal{H}(R - r) \quad \Rightarrow \quad \vec{\nabla}c = (-c_t\delta(R - r), 0) \quad (12)$$

where $\mathcal{H}$ is the Heaviside step function and δ the Dirac delta function, and we have switched to the standard polar coordinates (r, θ).

D. Boundary conditions

In the regions where the drag coefficient is constant, i.e., inside and outside of the OWF, we can write the equation for ψ as

$$K_{yy}\frac{\partial^2\psi}{\partial x^2} - 2K_{xy}\frac{\partial^2\psi}{\partial x\partial y} + K_{xx}\frac{\partial^2\psi}{\partial y^2} = 0. \tag{13}$$

The two solutions of (13) in these regions can then be connected by applying the jump conditions of (i) continuous streamlines, and (ii) integrating the full equation across the OWF boundary (see below and Appendix A). Note that the equation (13) remains elliptic regardless of the tidal parameters, since $K_{xy}^2/(K_{xx}K_{yy}) < 1$ always.

In addition to the jump conditions, a far-field boundary condition will be applied that requires the flow to approach that of an undisturbed free stream far from the OWF. Mathematically, this is represented as

$$\psi(x,y) \to \mathrm{Im}\{Ue^{-i\lambda_0}z\} \quad \text{as} \quad |z| \to \infty \tag{14}$$

with $z \equiv x + iy$, U denoting the magnitude of the free stream flow, and λ_0 the angle that the free stream makes to the horizontal.

III. ISOTROPIC TIDAL FRICTION – LINEAR DRAG

This section describes the method of solution for the problem by looking first at the simplest case so that we build up to the full solution stepwise. We therefore look at the situation where the friction tensor is what we will refer to as isotropic, being proportional to the identity matrix, i.e., where $K_{xy} = 0$ and $K_{xx} = K_{yy}$. This situation occurs when the tidal currents are circular with $\tilde{b} = 1$; having no preferred orientation. This is equivalent to representing the friction by a linear drag law, as in Garrett and Cummins [21].

A. Problem definition

The governing equation (9) then reduces to

$$c\nabla^2\psi + \vec{\nabla}c \cdot \vec{\nabla}\psi = 0. \tag{15}$$

It is important to note that this equation, together with our chosen form for the friction coefficient, results in a singular delta function behaviour of the second term on the OWF boundary at $r = R$, whereas Laplace's equation applies everywhere else in the domain, i.e.,

$$\nabla^2 \psi = 0 \quad \text{for } r \neq R. \tag{16}$$

To connect the two solutions in the regions inside and outside the OWF we apply the jump conditions.

The first of these jump conditions corresponds to the continuity of streamlines, i.e.,

$$\left[\!\left[\psi\right]\!\right]_R = 0, \tag{17}$$

where we use the notation that $\left[\!\left[f(x)\right]\!\right]_X \equiv f(X^+) - f(X^-)$. The second jump condition is described and derived in the appendix, and can be stated as

$$\left[\!\left[c\psi_r\right]\!\right]_R = 0. \tag{18}$$

Here, and henceforth, all subscripts on ψ denote partial derivatives.

It will be advantageous to use the complex potential function to derive solutions. This is defined as

$$\Omega(z) \equiv \Phi(x, y) + i\psi(x, y) \tag{19}$$

a function of the complex variable $z \equiv x + iy$. We will be concerned exclusively with the stream function (opposed to Φ), obtained through $\psi = \mathrm{Im}\{\Omega\}$. Using the results of complex variable theory we can also relate Ω to the velocity through

$$\frac{\mathrm{d}\Omega}{\mathrm{d}z} = \psi_y + i\psi_x = u - iv. \tag{20}$$

B. Solution

We will immediately write a general solution to the problem of the following form

$$\Omega(z) = Az + \begin{cases} \tau z + R^2\bar{\tau}/z & , z\bar{z} > R^2 \\ B & , z\bar{z} < R^2 \end{cases} \tag{21}$$

where A, B, τ are arbitrary complex constants to be determined by applying the jump and boundary conditions, and the overbar represents a complex conjugate.

First, we require that the streamlines are continuous across the OWF boundary at $r = R$ and find

$$\left[\!\left[\Omega\right]\!\right]_R = R(\tau e^{i\theta} + \overline{\tau e^{i\theta}}) - B, \tag{22}$$

with $z = Re^{i\theta}$. This shows that when B is taken to be real there is no jump in ψ across the boundary. Next, we require that the flow be uniform with velocity U, and at an angle of λ_0 to the horizontal, far from the OWF. This is written mathematically as

$$\Omega \to Ue^{-i\lambda_0} z \quad \text{for} \quad |z| \to \infty. \tag{23}$$

Applying this condition to the solution in (21) gives an expression for A,

$$(A + \tau)z = Ue^{-i\lambda_0} z \quad \Rightarrow \quad A = Ue^{-i\lambda_0} - \tau. \tag{24}$$

Finally, we can solve for the last remaining constant, τ, by applying the final jump condition. We do this by noting that the radial derivative of ψ can be expressed as

$$\psi_r = \mathrm{Im}\Big(e^{i\theta}\frac{\mathrm{d}\Omega}{\mathrm{d}z}\Big) \tag{25}$$

so that the jump condition can be found using

$$\frac{\mathrm{d}\Omega}{\mathrm{d}z} = Ue^{-i\lambda_0} - \begin{cases} R^2\bar{\tau}/z^2 & , z\bar{z} > R^2 \\ \tau & , z\bar{z} < R^2 \end{cases} \tag{26}$$

We can therefore write

$$e^{i\theta}\left[\!\left[c\,\mathrm{d}\Omega/\mathrm{d}z\right]\!\right]_R = (1+q)\tau e^{i\theta} - \overline{\tau e^{i\theta}} - qUe^{-i\lambda_0}e^{i\theta} \tag{27}$$

where we have defined the friction ratio $q \equiv c_t/c_0$. After taking the imaginary component of this and setting it to zero we can solve for τ as

$$\tau = \frac{q}{2+q} Ue^{-i\lambda_0}. \tag{28}$$

The full solution can then be written as follows

$$\Omega(z) = Ue^{-i\lambda_0} \cdot \begin{cases} z + \frac{q}{2+q} e^{i2\lambda_0} R^2/z & , z\bar{z} > R^2 \\ \frac{2}{2+q} z + B & , z\bar{z} < R^2 \end{cases} \tag{29}$$

with $\psi(x, y) = \mathrm{Im}\{\Omega\}$. Furthermore, the velocities of this solution can be easily computed through $u = \mathrm{Re}\{\mathrm{d}\Omega/\mathrm{d}z\}$ and $v = -\mathrm{Im}\{\mathrm{d}\Omega/\mathrm{d}z\}$.

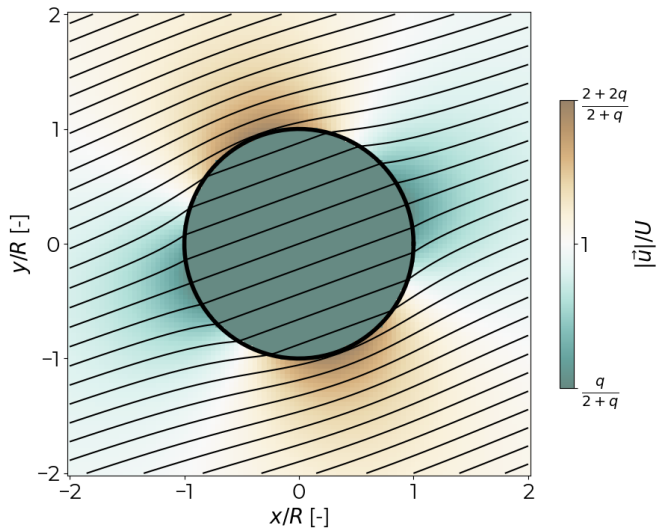

FIG. 1. Solution of the case of linear friction for the blocking effects in an OWF area ($r < R$) with boundary delineated by the thick black line. The lines show contours of the stream function. The ratio of the linear drag coefficients in this example is $q = c_t/c_0 = 3/4$ and the far-field flow has $\lambda_0 = 20°$. The colours show the magnitude of the velocity relative to the free stream, i.e., $|\vec{u}|/U$.

There are some interesting aspects of this solution that we now discuss. First, a solution is plotted in figure 1 for the value of $q = 3/4$, a value significantly larger than typical OWF conditions (see Table I) which we have chosen for illustrative purposes. It shows the streamlines of the flow diverging as they approach the OWF area and converging again symmetrically downstream.

We formulate the reduction in currents within the OWF by

$$\text{Reduction} \equiv 1 - \frac{\sqrt{u^2 + v^2}}{U}, \tag{30}$$

for $r < R$. This definition allows for values between zero and unity that correspond to no reduction and complete blocking, respectively. We find that this can be expressed through a function of the friction ratio as

$$\text{Reduction} = \frac{q}{2 + q}. \tag{31}$$

Note that these values are independent of the size R, of the OWF. They also have the expected limits: as $q \to 0$ there is no reduction of the currents, whereas for $q \to \infty$ there is a complete blocking of the flow with reductions of unity.

In addition to the current reduction within the OWF region, there is also an increase in current speed as the flow passes around the OWF (figure 1). The magnitude of this increase is greatest on the boundary of the OWF that is perpendicular to the free stream flow direction (i.e., at locations of $z = Re^{i(\lambda_0 \pm \pi/2)}$). The increase can be quantified to be equal in magnitude to the reduction, with the maximum and minimum velocities found to be $|\vec{u}|_{\max,\min}/U = 1 \pm q/(2+q)$.

The solution exhibits some unrealistic features that are a result of our simplifying assumptions. Most notably, the currents are found to be entirely horizontal and constant within the farm. This generally results in a jump in velocity across the farm boundary. In reality this sudden change will be spread out over a transition region that is set by the wakes of the individual structures.

IV. ANISOTROPIC TIDAL FRICTION

The full anisotropic tidal friction tensor is now used in finding a solution for mean flows with friction affected by general elliptic tidal currents. The solutions will then, generally depend on the additional tidal parameters describing the orientation ($\tilde{\theta}$) and degree of ellipticity ($\tilde{b}$).

A. Solution method by coordinate transformations

The approach that we take to obtain the solution of (9-12, 14) is through a series of three coordinate transformations. These are summarised in figure 2 and described in turn below.

1. The first coordinate transformation is designed to transform the governing equation (13), in the complex $z \equiv x + iy$ plane, into the Laplace equation in the $\xi \equiv \zeta + i\eta$ plane. This transformation is given by

$$\xi = bx + i(ax + y) \quad \text{with inverse} \quad z = \zeta/b + i(\eta - \frac{a}{b}\zeta) \tag{32}$$

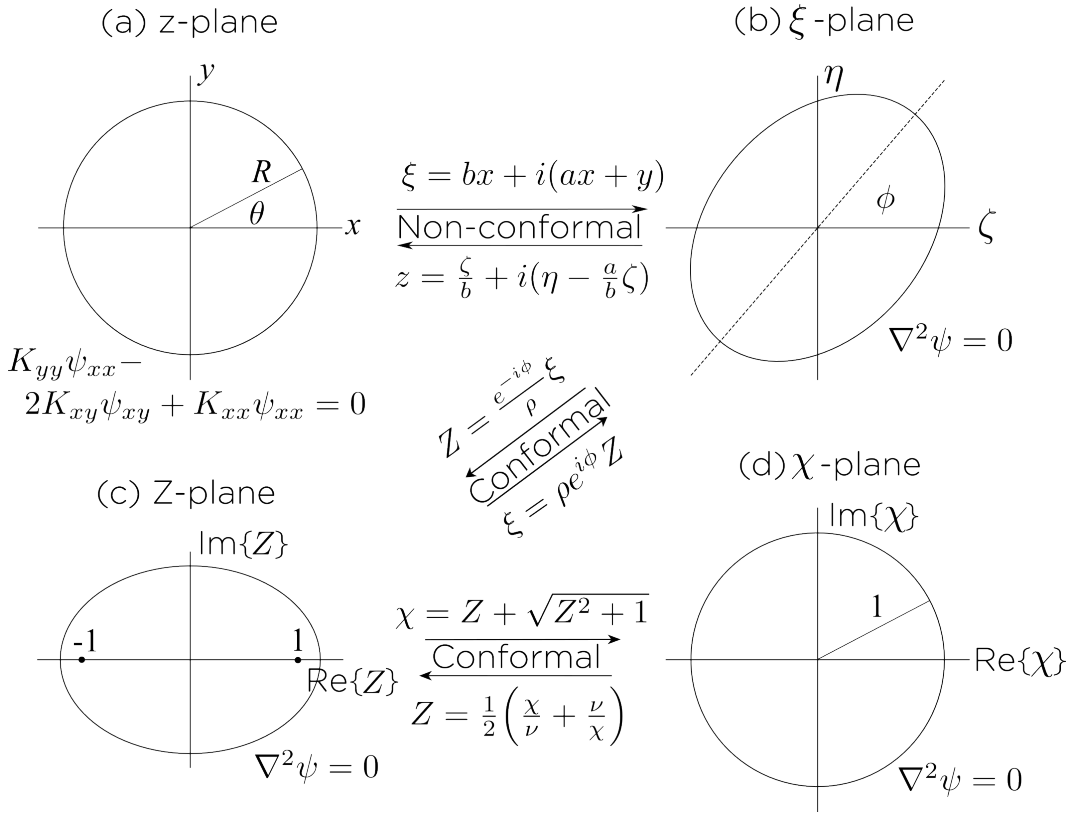

FIG. 2. Illustration of the sequence of transformations used in the solution of the anisotropic friction cases. Important parameters and scales are also shown, along with the governing equation of ψ in each domain away from the OWF boundary.

where

$$a \equiv K_{xy}/K_{yy} \quad \text{and} \quad b \equiv \Big(\frac{K_{xx}K_{yy} - K_{xy}^2}{K_{yy}^2}\Big)^{1/2}. \tag{33}$$

It can be written in terms of complex variables as

$$\xi = \Big(\frac{b+1}{2} + i\frac{a}{2}\Big)z + \Big(\frac{b-1}{2} + i\frac{a}{2}\Big)\bar{z} \equiv \gamma_+ e^{i\alpha_+} z + \gamma_- e^{i\alpha_-}\bar{z} \tag{34}$$

with inverse transformation of

$$z = \Big(\frac{1+b}{2b} - i\frac{a}{2b}\Big)\xi + \Big(\frac{1-b}{2b} - i\frac{a}{2b}\Big)\bar{\xi} = \frac{1}{b}\Big(\gamma_+ e^{-i\alpha_+}\xi - \gamma_- e^{i\alpha_-}\bar{\xi}\Big). \tag{35}$$

It may be verified that this coordinate system transforms (13) into Laplace's equation in the ξ-plane, i.e., $\psi_{\zeta\zeta} + \psi_{\eta\eta} = 0$. We note that this transformation is not conformal.

The boundary of a circlular OWF with radius R in the z-plane is transformed into a tilted ellipse in the ξ-plane. With the circle parameterised by $z = Re^{i\theta}$ this ellipse has

the equation

$$\xi(\theta) = Rb\cos\theta + iR(a\cos\theta + \sin\theta) \tag{36}$$

$$= R\Big(\frac{b+1}{2} + i\frac{a}{2}\Big)e^{i\theta} + R\Big(\frac{b-1}{2} + i\frac{a}{2}\Big)e^{-i\theta} \tag{37}$$

$$= R\gamma_+ e^{i(\theta+\alpha_+)} + R\gamma_- e^{-i(\theta-\alpha_-)} \tag{38}$$

where we have defined $2\gamma_\pm \equiv (a^2 + b^2 \pm 2b + 1)^{1/2}$, and have also $\tan\alpha_\pm \equiv a/(b \pm 1)$.

2. The second coordinate transformation is chosen as a rotation and scaling of the ellipse to place its focii in the Z-plane at $Z = \pm 1$. It is given by

$$Z = \frac{e^{-i\phi}}{\rho}\xi, \tag{39}$$

with coefficients of

$$\tan(2\phi) = \frac{2ab}{b^2 - a^2 - 1} \quad \text{and} \quad \rho = R(A'^{-1} - C'^{-1}) \tag{40}$$

with

$$A' = \frac{1+a^2}{b^2}\cos^2(\phi) - \frac{a}{b}\sin(2\phi) + \sin^2(\phi), \quad C' = \frac{1+a^2}{b^2}\sin^2(\phi) + \frac{a}{b}\sin(2\phi) + \cos^2(\phi). \tag{41}$$

Note that because this transformation is conformal Laplace's equation must be satisfied in the Z-plane. The ellipse has the equation

$$Z(\theta) = \frac{R}{\rho}e^{-i\phi}[b\cos\theta + i(a\cos\theta + \sin\theta)] \tag{42}$$

$$= \frac{R}{\rho}[\gamma_+ e^{i(\theta+\beta)} + \gamma_- e^{-i(\theta+\beta)}] \tag{43}$$

in the complex Z-plane, where $2\beta \equiv \alpha_+ - \alpha_-$, and $2\phi = \alpha_+ + \alpha_-$. It is possible to show that $\beta = -\tilde{\theta}$, i.e., the negative of the orientation of the major axis of the tidal currents (see Appendix for derivation). The Z-plane ellipse can be seen to have major and minor axes given by $2\frac{R}{\rho}(\gamma_+ + \gamma_-)$ and $2\frac{R}{\rho}(\gamma_+ - \gamma_-)$, respectively.

3. The final coordinate transformation takes the ellipse in the Z-plane to the unit circle in the χ-plane via

$$\chi = \nu(Z + \sqrt{Z^2 - 1}) \tag{44}$$

with

$$\nu = \frac{R}{\rho\sqrt{A'}} - \sqrt{\frac{R^2}{\rho^2 A'} - 1}. \tag{45}$$

It is also conformal so that the stream function satisfies the Laplace equation in the χ-plane. Care must be taken in this transform to choose the correct branch cuts in the square root term. The branch cut must be placed on the line between $Z = \pm 1$. The inverse transform is given by

$$Z = \frac{1}{2}\Big(\frac{\chi}{\nu} + \frac{\nu}{\chi}\Big). \tag{46}$$

Relationships between ν and other parameters can be derived by substituting $\chi(\theta - \tilde{\theta})$ into the above equation for Z and equating the major and minor axes lengths to give $2\frac{R}{\rho}(\gamma_+ \pm \gamma_-) = \nu \pm \nu^{-1}$. For example, we can find that $2\frac{R}{\rho}\gamma_+ = \nu$ and $2\frac{R}{\rho}\gamma_- = \nu^{-1}$.

Now that these transformations are in place we can specify the solution for Laplace's equation in the χ-plane and then perform the inverse transformations to recover the solution in the original z-plane.

B. Solution for infinite q

This special case consists of the limit as $q \to \infty$ so that the circular OWF can be treated as a solid object. There is only one solution that applies outside the OWF area, and one boundary condition needed on the OWF boundary, namely that it must be a streamline, i.e., $\psi = 0$ on $r = R$.

The solution for flow around a unit circular cylinder can be expressed in the χ-plane as

$$\Omega(\chi) = \tau\chi + \frac{\bar{\tau}}{\chi}, \tag{47}$$

for some appropriately chosen complex constant τ. Notice that on the unit circle we have $\chi\bar{\chi} = 1$ and Ω becomes the sum of two complex conjugate terms. This shows that the unit circle is the $\psi = 0$ streamline, and it can be confirmed that this boundary condition is also satisfied in the z-plane.

The final boundary condition is that the correct far-field flow is obtained. To do this, we look at how the uniform flow in the z-plane can be transformed to a condition in the χ-plane. Given the general uniform flow of $\Omega(x, y) = Ue^{-i\lambda_0}z$, we can write this in the ξ-plane as

$$\Omega(\zeta, \eta) = \frac{U}{b}e^{-i\lambda_0}[\zeta + i(b\eta - a\zeta)]. \tag{48}$$

However, it can be seen that this complex potential cannot be written as a function of ξ only, i.e., we must write $\Omega = \Omega(\xi, \bar{\xi})$ since the transformation between the z- and ξ-planes is not conformal. To avoid use of the conjugate in the conformal transformations to follow, we express the complex potential in the ξ-plane in terms of an "equivalent" potential

$$\Omega^*(\xi) = U\gamma e^{-i\lambda_1}\xi, \tag{49}$$

defined such that the imaginary (stream function) part gives the correct far-field flow upon transformation back to the z-plane. It can be shown that

$$\gamma = [(a\cos\lambda_0 + \sin\lambda_0)^2 + (b\cos\lambda_0)^2]^{1/2}/b \quad \text{and} \quad \tan(\lambda_1) = \frac{a\cos\lambda_0 + \sin\lambda_0}{b\cos\lambda_0}. \tag{50}$$

It is now straight forward to match this uniform flow in the far-field with a condition in the χ-plane; as $|z| \to \infty$ we have also all of $|\xi|, |Z|, |\chi| \to \infty$, so

$$\xi \to \frac{\rho}{2\nu}e^{i\phi}\chi \quad \Rightarrow \quad \Omega^* \to \frac{U\gamma\rho}{2\nu}e^{i(\phi-\lambda_1)}\chi. \tag{51}$$

We can therefore equate the coefficient of the first (far-field) term of (47) with (49,51) to give

$$\tau = \frac{U\gamma\rho}{2\nu}e^{i(\phi-\lambda_1)}, \tag{52}$$

and a full solution of

$$\Omega(\chi) = \frac{U\rho\gamma}{2\nu}\Big[\chi e^{-i(\lambda_1-\phi)} + \frac{e^{i(\lambda_1-\phi)}}{\chi}\Big]. \tag{53}$$

The imaginary part of this solution, giving the streamlines, is plotted in Fig. 3 for a specific example. Note that we have also included the field inside the OWF, which in this case of infinite friction is not a part of the solution domain. It is included only for mathematical insight since it shows the position of the branch cut.

The solution in Fig. 3 shows that the symmetry of the classical flow around a cylinder is broken with the introduction of the anisotropic friction tensor. This is best manifest through the shifting of the stagnation points on the cylinder surface through the angle $\theta_{\rm sp}$. By setting $\mathrm{d}\Omega/\mathrm{d}\chi = 0$ on the surface of the cylinder, we can solve for the locations of the stagnation points as $\theta_{\rm sp} = \lambda_1 - \phi + \tilde{\theta}$ with $\pm\pi$ radians added to this to get the second stagnation point. The stagnation point locations are a function only of the tidal ellipse parameters $\tilde{b}, \tilde{\theta}$, and Fig. 4 shows how they change the value of $\theta_{\rm sp}$: the more rectilinear the tidal currents (i.e. lower $\tilde{b}$), and the closer to 50° the ellipse orientation (for low $\tilde{b}$), the larger the stagnation point angle. However, they do not reach larger than ±10° from the far-field current direction.

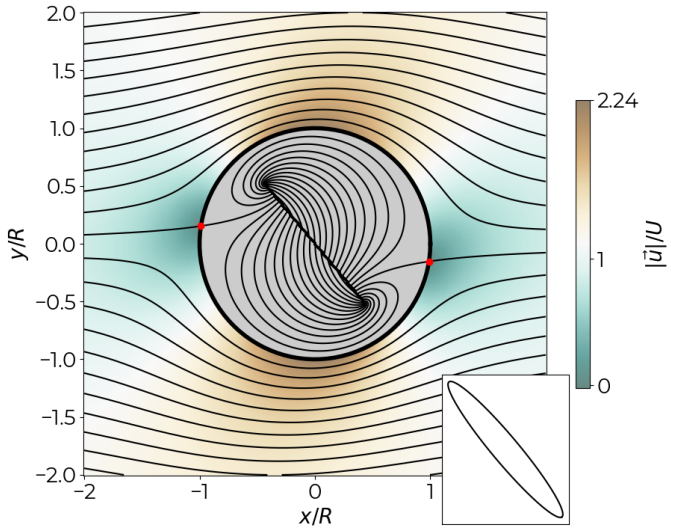

FIG. 3. Streamlines of flow past a circular OWF in the limit of infinite friction, i.e., $q \to \infty$. Streamlines within the OWF region are not part of the physical domain, and are only plotted for mathematical insight. The tidal current ellipse is plotted in the lower right inset panel with parameters of $\tilde{b} = 0.15$, $\tilde{\theta} = 60°$, and $\lambda_0 = 0°$. Stagnation points on the cylinder are shown as red dots with colours representing the velocity magnitude as in figure 1.

C. Anisotropic tidal friction – the full problem

Similar to our approach in the last two subsections, here we apply the same coordinate transformations and propose a trial solution of a similar form, i.e. we let

$$\Omega = AZ + \begin{cases} \tau\chi + \bar{\tau}/\chi & , \chi\bar{\chi} > 1 \\ B & , \chi\bar{\chi} < 1 \end{cases}, \tag{54}$$

with A, B, τ complex constants. We also write this trial solution as $\Omega = \Omega_0(Z) + \Omega_1(\chi)$ with $\Omega_0 = AZ$ defined throughout the domain, and Ω_1 (the final term in Eq 54) defined differently inside and outside the OWF area. The $\Omega_0(Z)$ part is not explicitly written in terms of χ to avoid an unnecessary singularity in the χ-plane [23]. To arrive at a solution we now apply each of the jump and boundary conditions to solve for the constants.

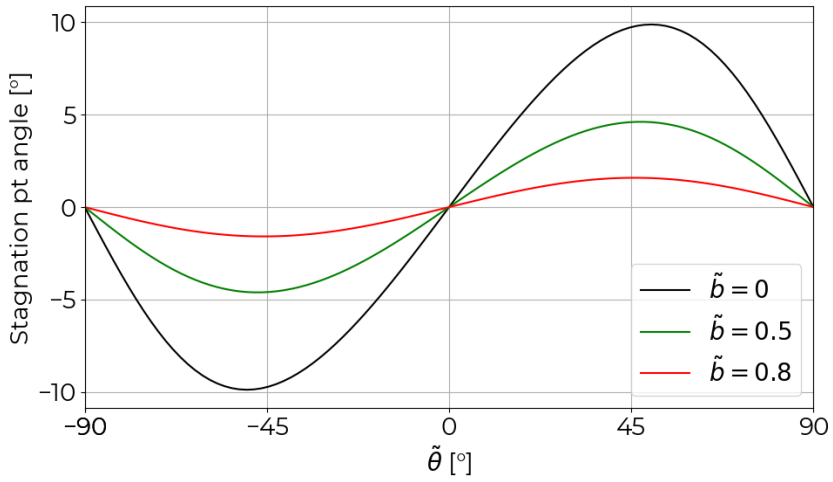

FIG. 4. Angle of the stagnation points, θ_{sp}, as a function of the tidal ellipse parameters.

Jump condition 1 – Continuous streamlines

The jump condition that requires continuous streamlines is easily fulfilled if we choose B to be real, since on the boundary $\chi\bar{\chi} = 1$ and inside and outside the OWF boundary Ω_1 has vanishing imaginary component. For simplicity we set $B = 0$.

The far-field boundary condition

In applying the far-field boundary condition from (51) to our trial solution (54) we are able to solve for A in terms of τ as

$$A = U\gamma\rho e^{i(\phi-\lambda_1)} - 2\nu\tau. \tag{55}$$

It can be seen that the second term above is chosen to exactly cancel the far-field contribution of $\Omega_1(\chi)$, with the first term then providing the correct "equivalent" potential to result in the required far-field flow (exactly as in the linear drag case).

Jump condition 2

The final coefficient τ, can be determined from the second jump condition. It is helpful to split the solution for ψ into two components associated with the two terms of $\Omega = \Omega_0 + \Omega_1$

so that $\psi = \psi^0 + \psi^1$, with ψ^1 being valid outside the OWF region only. This can then be substituted into the jump condition found in the appendix of

$$m\left[\!\left[c\psi_r\right]\!\right]_{r=R} - \frac{nc_t}{R}\psi_\theta\Big|_{r=R} = 0, \tag{56}$$

where $m \equiv k_{yy}\cos^2\theta - 2k_{xy}\sin\theta\cos\theta + k_{xx}\sin^2\theta$ and $n \equiv (k_{xx} - k_{yy})\sin\theta\cos\theta + k_{xy}(\sin^2\theta - \cos^2\theta)$. It is possible to simplify the jump condition above to

$$m\psi_r^1|_{r=R} = q[\psi_x^0(m\cos\theta - n\sin\theta) + \psi_y^0(m\sin\theta + n\cos\theta)], \tag{57}$$

and to substitute into ψ on both sides using the trial solution in (54). The radial gradient of ψ^1 on the left hand side can be written as

$$\psi_r = \cos\theta\psi_x + \sin\theta\psi_y = b\cos\theta\psi_\zeta + (a\cos\theta + \sin\theta)\psi_\eta. \tag{58}$$

This can then be combined with expressions for the gradients from the chain rule

$$\frac{\mathrm{d}\Omega_1}{\mathrm{d}\xi} = \psi_\eta + i\psi_\zeta = \frac{\mathrm{d}Z}{\mathrm{d}\xi}\frac{\mathrm{d}\chi}{\mathrm{d}Z}\frac{\mathrm{d}\Omega_1}{\mathrm{d}\chi}, \tag{59}$$

where each term can be calculated from the transformations and the trial solution as

$$\frac{\mathrm{d}Z}{\mathrm{d}\xi} = \frac{e^{-i\phi}}{\rho}, \quad \frac{\mathrm{d}\chi}{\mathrm{d}Z} = \frac{2\nu\chi^2}{\chi^2 - \nu^2}, \quad \frac{\mathrm{d}\Omega_1}{\mathrm{d}\chi} = \tau - \frac{\bar{\tau}}{\chi^2}. \tag{60}$$

Here we have expressed everything in terms of χ, and can write as

$$\frac{\mathrm{d}\Omega_1}{\mathrm{d}\xi} = \frac{2\nu}{\rho e^{i\phi}} \cdot \frac{\tau\chi^2 - \bar{\tau}}{\chi^2 - \nu^2}, \tag{61}$$

with the OWF boundary given in the χ-plane by the parametric equation $\chi(\theta) = e^{i(\theta - \tilde{\theta})}$.

Unfortunately, we were not able to find a managable closed form analytical solution to the jump condition equation (57-61), and have relied on a numerical solution for the results presented in the following. Details of the solution method are described in Appendix C.

Results

An example of the streamlines resulting from the above solution is shown in figure 5. There are two general features of the solution that are worth noting: (i) the reduction in current strength throughout the OWF, and (ii) a slight deflection of the current direction

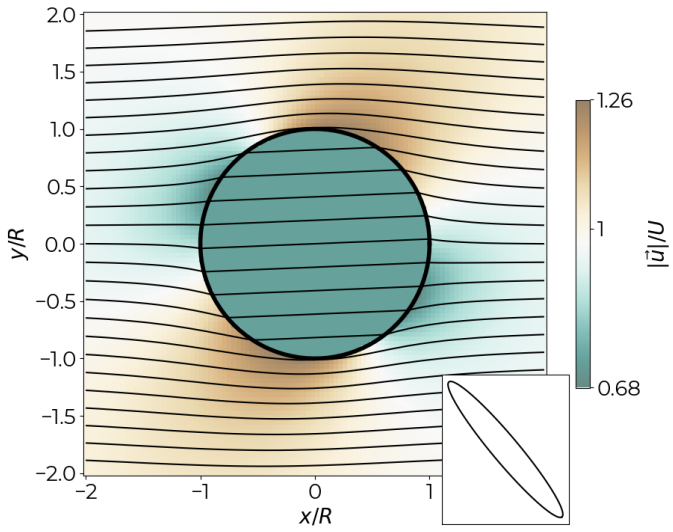

FIG. 5. Streamlines of flow past a circular OWF with the full anisotropic friction. Parameter values correspond to $q = 3/4$, $\tilde{\theta} = -50°$, $\tilde{b} = 0.15$, and $\lambda_0 = 0°$. The tidal ellipse is shown in the lower right inset. The flow within the OWF shows a reduction in current of 0.27 and a deflection of 2.1°.

within the OWF. The reduction was defined in (30) above, and the deflection is defined mathematically by

$$\text{Deflection} \equiv \tan^{-1}\left(\frac{v}{u}\right) - \lambda_0 \tag{62}$$

where $\vec{u} = (u, v) = (\psi_y, -\psi_x)$ is the flow within the OWF region, $r < R$. By first fixing the parameters describing the tidal ellipse ($\tilde{b}$, $\tilde{\theta}$), and the far-field flow angle ($\lambda_0 = 0$), both the reduction and deflection of the flow within the OWF area are plotted as a function of the friction coefficient, q, in figure 6. It can be seen that the reduction in current strength follows the linear drag solution of $q/(2+q)$, described in section III, very closely (figure 6a, dashed line). This result also holds when other values of $\tilde{b}$ and $\tilde{\theta}$ are chosen. As expected, the reduction in currents approaches unity as $q \to \infty$, and vanishes as $q \to 0$.

An additional aspect of the solution that arises when anisotropic friction is used, is the deflection of the currents within, and around, the OWF. This was first seen in the infinite

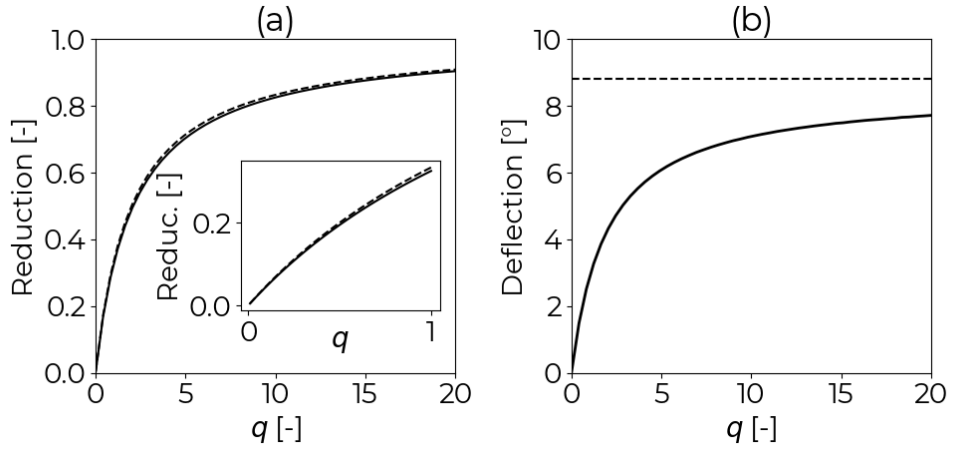

FIG. 6. The reduction (a) and deflection (b) of the flow within the OWF as a function of the friction coefficient, q. The dashed line in (a) is the linear friction result for the reduction in current strength given by $q/(2+q)$. The inset in (a) shows the reduction in the OWF-relevant range of q. The dashed line in (b) represents the stagnation point angle at infinite friction. Other parameters taken for these plots are $\tilde{b} = 0.15$, $\tilde{\theta} = -50°$, $\lambda_0 = 0°$.

friction case in section IV B for $q \to \infty$, where a shifting of the position of the stagnation points was found. As q increases in figure 6(b) we see the deflection of the flow within the OWF being bounded by this stagnation point value.

The dependence of the current reduction and deflection on the orientation of the tidal ellipse is plotted in figure 7. Here we have fixed $\tilde{b} = 0$, giving rectilinear tidal currents for which the largest deviations from the linear drag case are seen. Since the current reduction follows the $q/(2+q)$ scaling so closely, we have normalised the reduction by this amount to look at variation around this level in figure 7(a). The results show that $\tilde{\theta}$ can cause departures from the $q/(2+q)$ result by more than $\pm 10\%$, with the largest magnitudes found at the lowest OWF friction (q) levels, and at tidal current orientations that are parrallel (highest reduction) and perpendicular (smallest reduction) to the mean flow. Little deviation from the linear drag scaling result are seen when the tidal current orientation is at 45° to the mean flow (figure 7a). On the other hand, the deflection shows a maximum close to orientations of 45°, with trends of increasing deflection for increased friction ratio (figure 7b).

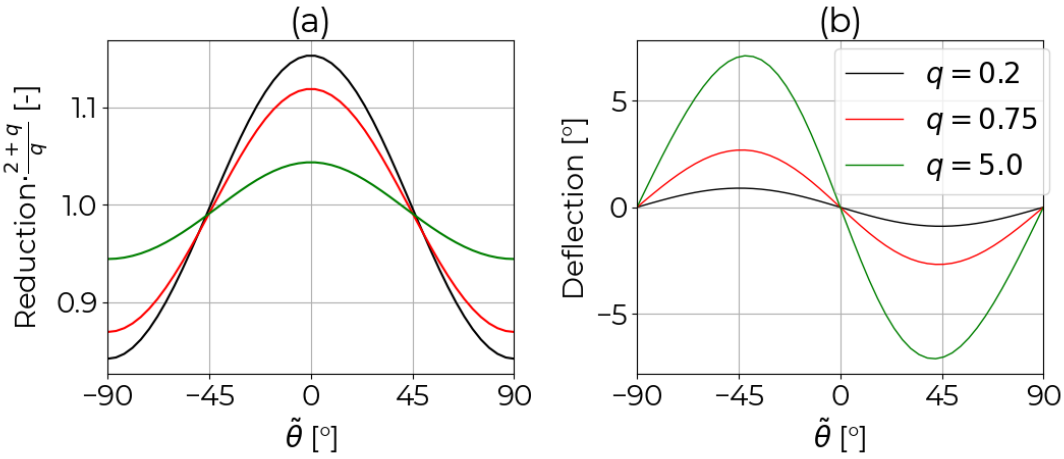

FIG. 7. The reduction (a) and deflection (b) of the flow within the OWF as a function of the tidal ellipse orientation, $\tilde{\theta}$. The reduction values in (a) have been normalised by the linear drag scaling of $q/(q+2)$. For all curves $\tilde{b} = 0$.

V. APPLICATION TO OWFS IN THE NORTH SEA

In this section, we tabulate typical parameters for three OWFs in the North Sea, and apply the solution described above to arrive at expected values of current reductions and deflections.

The friction ratios of typical OWFs can be expressed in terms of tabulated values, as in section II A, through

$$q \equiv \frac{c_t}{c_0} = \frac{C_D^t}{2C_D^0} \cdot \frac{A_f}{\ell^2}. \tag{63}$$

We find it helpful to think of q as being composed of the product of two terms (as formatted in equation 63 above). The first being a simple ratio of drag coefficients for the OWF foundation structures and the flat sea bed, with much higher drag coefficients associated with the separated wakes of the cylindrical foundation structures than the bottom boundary layer of the sea bed. However, this larger structure drag coefficient factor is outweighed by the second factor, the ratio of the structure frontal area to the area of sea bed around a foundation structure (ℓ^2). The resulting values of q are then typically well below unity. For the BARD 1 and Global Tech OWFs in the southern North Sea, Carpenter et al. [14] have estimated these areas and drag coefficients, and using their values we find $q = 0.11$ for

BARD 1 and $q = 0.21$ for Global Tech (Table I). Very different friction ratios can be found in the Dogger Bank group of OWFs, where a relatively wide spacing of the monopile turbine foundations ($\ell \approx 2.4$ km) leads to a very low $q = O(0.01)$. A summary of the relevant parameter estimates for the Dogger Bank OWFs (Dogger Bank A, B, C, and Sophia, which are still being installed at this time), which we group together, are presented in Table I.

The tidal currents and mean flows at the OWF sites are derived from regional simulations designed to study the effects of OWFs on North Sea oceanography, as described in Christiansen et al. [12, 19]. They have currents that are dominated by the M2 tidal component with values that characterise the tidal ellipse, and the mean flow shown in Table I. All other tidal components have been neglected for simplicity, but can easily be accounted for in the computation of the tidal friction tensor. From the parameters in Table I we can verify the assumption that the tidal currents are much larger than the mean flow, i.e., $U/\tilde{u} < O(0.1)$ at all OWFs.

With the parameters listed in Table I we are able to make estimates of the reduction and deflection of the mean currents in an idealised OWF with similar friction, tidal, and mean flow parameters as those in Table I, but with our idealised circular geometry. Application of the model solution described in section IV C above results in mean flow current reductions of 0.048 and 0.086 in BARD and Global Tech, respectively, and deflections of less than one degree (see 'Model predictions' section of Table I). These estimates of the current reductions are within the range reported in [19], who use a drag-based increase of the bottom stress and turbulence production in a realistic simulation of OWFs in the North Sea. The current blocking effects of the Dogger Bank OWF however, are predicted to be negligible. This is due to the one order of magnitude smaller friction ratio that comes with the significantly larger foundation structure spacing, ℓ.

VI. DISCUSSION

Our derivation of the solution for blocking effects within, and around, OWFs has made some simplifying assumptions that are worth discussing in more detail. The first such assumption was the neglect of the nonlinear advection terms in (1). Following Garrett and Cummins [21], we evaluate the importance of the nonlinear terms through an order of magnitude analysis, comparing them to the friction term. Noting that the nonlinear terms

are expected to scale with the tidal velocity, $\tilde{u}$, and the length scale of the OWF, R, we find $\vec{u}\cdot\nabla\vec{u} \sim \tilde{u}^2/R$. Similarly, the friction term is $C_D^0\tilde{u}^2/H$. Taking the ratio of these two terms, for our assumption to hold we require the dimensionless number

$$\xi \equiv \frac{H}{C_D^0 R} \ll 1. \tag{64}$$

Substituting in for each quantity in ξ for the BARD and Global Tech OWFs from Table I, and choosing a representative $R = 10$ km, gives the estimate of $\xi = O(1)$. Therefore, we expect that the nonlinear terms could play a role in the dynamics of these OWFs at their current sizes. As the size of OWFs grows in the future, this will have the effect of reducing ξ to limit the nonlinear effects. In the Dogger Bank OWF we find lower values in the range of $\xi = 0.3 - 0.6$.

Even if we considered only cases with $\xi \ll 1$, the neglect of the nonlinear terms is not universally valid throughout the solution domain. In particular, we have assumed above that the length scale of variability in the solution is R, whereas the actual solution shows rapid variability at the OWF boundary (figure 5). In these regions a full solution would give a smooth transition across the boundary.

Another simplifying assumption that was made in deriving the solution was to neglect any feedbacks between the increased friction of the OWF and the tidal currents. This is also expected to be accurate if the friction term is not of leading order in the balance of the tidal currents. We assess this by comparing the magnitude of the unsteady term for an M2 tidal forcing, $\partial\vec{u}/\partial t \sim \tilde{u}\omega_{M2}$, with ω_{M2} the angular frequency of the M2 tide, to the friction term of the tidal currents, $C_D^0\tilde{u}^2/H$. Using the typical values listed above, we find the unsteady term to be a factor of approximately 5 larger. We therefore expect that the introduction of increased friction from the OWFs does not lead to large changes in tidal currents, as found in Cazenave et al. [20].

VII. CONCLUSIONS

An idealised model has been developed of the process by which the increased frictional drag of offshore wind farms (OWFs) creates a 'blocking' of mean ocean currents. This was done by extending the previous work of Garrett and Cummins [21] to allow for a modified 'anisotropic' friction that arises from the quadratic drag law in the presence of

strong elliptical tidal currents. The modification requires that a series of transformations be made to convert the elliptical partial differential equation to Laplace's equation, and into a circular geometry that can be solved with known solutions.

The results predict that for typical values of OWF foundation structures in the southern North Sea, the reduction of mean current magnitudes within the farms can be up to approximately 10%, depending on the relatively uncertain drag coefficient of the foundation structures. This result is in line with a recent study by Christiansen et al. [19], despite the idealised circular geometry of the OWF and the neglect of nonlinear effects. The model thus provides theoretical guidance to understand the possible alteration of mean currents on the continental shelves where OWFs are installed, or planned. The model is expected to apply to shelf seas where there is no strong feedback between changes in bottom friction and tidal currents, and in cases where the nonlinear terms are small. In future OWF scenarios where larger farms are envisioned to be placed in deeper waters, the nonlinear terms are expected to be less important.

The results show that reductions in mean currents are primarily a function of the ratio of friction coefficients, q, between inside and outside the OWF, and scales similar to the linear drag law result, i.e., with reduction $\sim q/(2+q)$. This relation can be expressed directly in terms of estimated OWF parameters as a reduction of $C_D^t/(4C_D^0\ell^2/A_f + C_D^t)$ in the mean currents, with dependence on both the drag coefficients (structure and sea bed) and the area ratio of the OWF structures and their spacing. Typical values for the reductions in current scenarios of OWF development show that the current reductions are likely less that 10%, and show large variability depending on the density and geometry of the structures in individual OWFs, where current reductions can also be negligible. Additional dependence on the tidal ellipse parameters is also found, and can amount to deviations from this scaling of more than 10%, especially at low q. In addition to a current reduction, there may also be a deflection of the current inside the OWF, however, these angles of deflection are small ($< 1^\circ$) for expected levels of q, with theoretical maximum deflections of $< 10^\circ$ for large q.

With our focus on a purely circular OWF geometry we have neglected to include a parameter that describes a *farm* orientation. Such a parameter should have an effect on the current field. In particular, we note that many OWF installations and development plans have a polygon shape which may be possible to develop numerical solutions for using the model derived herein. This is left for potential future work, which should also focus on the

influence of the nonlinearity parameter. We recommend conducting intermediate studies, between the idealised model presented herein and the realistic simulations of Christiansen et al.[19], that focus on the response of OWFs with realistic geometries and nonlinear effects.

ACKNOWLEDGMENTS

Support of JRC by the Helmholtz Association through the PoF-IV programme is gratefully acknowledged. We also thank Nils Christiansen for his comments and support in quantifying North Sea tidal currents.

Appendix A. Derivation of the jump condition

As described above, the second jump condition that must be applied is derived by integrating the full equation $\hat{k} \cdot (\vec{\nabla} \times \mathbf{K}\vec{u}) = 0$, across the OWF boundary, where gradients of $c(x, y)$ are singular with delta function behaviour. In terms of the stream function, we write this as

$$c\vec{\nabla} \cdot (\mathbf{k}^* \vec{\nabla}\psi) + \vec{\nabla} c \cdot (\mathbf{k}^* \vec{\nabla}\psi) = 0, \tag{65}$$

which correspond to the L_1 and L_2 operator terms in (9). Here we have defined

$$\mathbf{k}^* \equiv \begin{bmatrix} -k_{yy} & k_{xy} \\ k_{xy} & -k_{xx} \end{bmatrix}. \tag{66}$$

These terms can be combined into

$$\vec{\nabla} \cdot (c\, \mathbf{k}^* \vec{\nabla}\psi) = 0. \tag{67}$$

We then integrate this equation over some part of the domain, V, and apply the divergence theorem to show

$$\int_V \vec{\nabla} \cdot (c\vec{A}) dV = \int_{\partial V} c\vec{A} \cdot \hat{n} dS = 0, \tag{68}$$

where we denote $\vec{A} \equiv \mathbf{k}^* \vec{\nabla}\psi$, and $\hat{n}$ the unit normal to the boundary ∂V. Since ∂V can be taken anywhere in the domain, we set it equal to the outside and inside of the OWF boundary, denoted $\Gamma^{\pm}$ respectively. Then we can write

$$\int_{\Gamma^+} c\vec{A} \cdot \hat{n} dS - \int_{\Gamma^-} c\vec{A} \cdot \hat{n} dS = 0 \tag{69}$$

so that taking the curves $\Gamma^{\pm}$ infinitely close together leads to

$$\left[\!\left[c\vec{A}\cdot\hat{n}\right]\!\right]_{\Gamma}=0, \tag{70}$$

and the general form for the jump condition of

$$\left[\!\left[c\,\mathbf{k}^{*}\vec{\nabla}\psi\cdot\hat{n}\right]\!\right]_{\Gamma}=0. \tag{71}$$

This can alternatively be expressed in the form

$$\left[\!\left[c\,\mathbf{k}\vec{u}\cdot\hat{\tau}\right]\!\right]_{\Gamma}=0, \tag{72}$$

where $\hat{\tau}$ is the unit tangent vector to the surface Γ. This form of the general jump condition in (72) has a simple physical interpretation, namely, that the tangential component of the frictional stress is continuous across the OWF boundary. This can be seen from the fact that the frictional stress is proportional to $c\,\mathbf{k}\vec{u}$ from (5).

We can verify that this general form produces the correct results in specific cases. In the case of linear friction with a circular OWF of radius R this becomes

$$\left[\!\left[c\psi_{r}\right]\!\right]_{R}=0, \tag{73}$$

in agreement with [21].

For the same circular OWF where the friction is anisotropic, we can express

$$(\mathbf{k}^{*}\vec{\nabla}\psi)\cdot\hat{n}=-k_{yy}\cos\theta\psi_{x}+k_{xy}\cos\theta\psi_{y}+k_{xy}\sin\theta\psi_{x}-k_{xx}\sin\theta\psi_{y} \tag{74}$$

and after switching to polar coordinates, this gives

$$(\mathbf{k}^{*}\vec{\nabla}\psi)\cdot\hat{n}=-m\psi_{r}-n\frac{\psi_{\theta}}{r}. \tag{75}$$

Then accounting for the jump across $r=R$ we get the final form of the jump condition of

$$m\left[\!\left[c\psi_{r}\right]\!\right]_{R}-\frac{c_{t}n}{R}\psi_{\theta}(R,\theta)=0. \tag{76}$$

This form can alternatively be derived directly from (9) by substituting for the polar forms of the second derivatives and integrating across $r=R$ and using integration by parts.

Appendix B. Derivation of $\beta = -\tilde{\theta}$

Using the following identity

$$\tan^{-1} x - \tan^{-1} y = \tan^{-1}\left(\frac{x-y}{1-xy}\right) \tag{77}$$

we can write

$$2\beta = \alpha_+ - \alpha_- = \tan^{-1}\left(\frac{-2a}{a^2+b^2-1}\right) \tag{78}$$

then we will substitute in for a, b using their definitions in terms of the $\mathbf{k}$ components. It is helpful to explicitly write the tensor components in terms of the tidal current ellipse orientation via

$$k_{xx} = \tilde{u}[g_1 - g_2 \sin^2(\tilde{\theta})] \tag{79}$$

$$k_{yy} = \tilde{u}[g_1 - g_2 \cos^2(\tilde{\theta})] \tag{80}$$

$$k_{xy} = \tilde{u}\frac{g_2}{2}\sin(2\tilde{\theta}) \tag{81}$$

with the coefficients g_i independent of $\tilde{\theta}$, and given by

$$g_0 \equiv \Big\langle \frac{\cos^2(\omega t)}{[\cos^2(\omega t) + \tilde{b}^2 \sin^2(\omega t)]^{1/2}} \Big\rangle, \quad g_1 = 3g_0 - g_2, \quad g_2 \equiv \Big\langle \frac{\cos^2(\omega t) - \tilde{b}^2 \sin^2(\omega t)}{[\cos^2(\omega t) + \tilde{b}^2 \sin^2(\omega t)]^{1/2}} \Big\rangle. \tag{82}$$

Then, substituting in (79-81) above leads to

$$\frac{-2a}{a^2+b^2-1} = \frac{-2k_{xy}}{k_{xx}-k_{yy}} = -\tan(2\tilde{\theta}). \tag{83}$$

After using the odd property of the inverse tangent function, this gives the desired result of $\beta = (\alpha_+ - \alpha_-)/2 = -\tilde{\theta}$.

Appendix C. Solving the jump condition for τ

The procedure that we use to solve the second jump condition (57) for τ is as follows. It can be shown through substitution of the k_{ij} that

$$m(\theta) = \tilde{u}\Big\{g_3 - \frac{g_2}{2}\cos[2(\theta - \tilde{\theta})]\Big\} \quad \text{and} \quad n(\theta) = \tilde{u}\frac{g_2}{2}\sin[2(\theta - \tilde{\theta})] \tag{84}$$

where we have defined $g_3 \equiv g_1 - g_2/2$. It is important to note that the RHS can be expressed as a purely sinusoidal function of θ (i.e. with unit frequency). This can be seen through the results that

$$m\cos\theta - n\sin\theta = \tilde{u}\Big[g_3\cos\theta - \frac{g_2}{2}\cos(\theta - 2\tilde{\theta})\Big] \tag{85}$$

$$m\sin\theta + n\cos\theta = \tilde{u}\Big[g_3\sin\theta + \frac{g_2}{2}\sin(\theta - 2\tilde{\theta})\Big], \tag{86}$$

combined with the fact that $\psi^0_{x,y}$ are constants. ψ^0 is the stream function of a uniform flow, given by

$$\psi_0(x,y) = U(y\cos\lambda_0 - x\sin\lambda_0) - \frac{2\nu}{\rho} Im\{\tau e^{-i\phi}\xi\} \tag{87}$$

It can be expanded to give the gradients in the z-plane of

$$\psi^0_x = -U\sin\lambda_0 - \tau_*\frac{2\nu}{\rho}[a\cos(\theta_* - \phi) + b\sin(\theta_* - \phi)] \tag{88}$$

$$\psi^0_y = U\cos\lambda_0 - \tau_*\frac{2\nu}{\rho}\cos(\theta_* - \phi), \tag{89}$$

where we have defined $\tau \equiv \tau_* e^{i\theta_*}$.

Looking at the LHS, it is useful to multiply top and bottom of (61) by the complex conjugate of the denominator and evaluate on the boundary (where $\chi\bar{\chi} = 1$) to get

$$\frac{\mathrm{d}\Omega_1}{\mathrm{d}\xi} = \frac{2\nu}{\rho e^{i\phi}} \cdot \frac{\nu(\tau/\nu + \bar{\tau}\nu - \overline{\tau\chi^2}/\nu - \nu\tau\chi^2)}{2\nu^2(\frac{1+\nu^4}{2\nu^2} - \cos[2(\theta - \tilde{\theta})])}. \tag{90}$$

But we can show that

$$\frac{1+\nu^4}{2\nu^2} = \frac{2g_1 - g_2}{g_2} \equiv g_4 \tag{91}$$

so that

$$\frac{1+\nu^4}{2\nu^2} - \cos[2(\theta - \tilde{\theta})] = \frac{2m}{\tilde{u}g_2}, \tag{92}$$

and finally we have

$$\frac{\mathrm{d}\Omega_1}{\mathrm{d}\xi} = \frac{g_2\tilde{u}}{2\rho m} e^{-i\phi}\Big(\frac{\tau}{\nu} + \bar{\tau}\nu - \frac{\overline{\tau\chi^2}}{\nu} - \nu\tau\chi^2\Big). \tag{93}$$

Substituting the above forms into the jump condition give us a LHS of

$$b\cos\theta \mathrm{Im}\{e^{-i\phi}f\} + (a\cos\theta + \sin\theta)\mathrm{Re}\{e^{-i\phi}f\} \tag{94}$$

where we have defined $f(\theta) \equiv \tau/\nu + \bar{\tau}\nu - \overline{\tau\chi^2}/\nu - \nu\tau\chi^2$, with $\chi = e^{i(\theta - \tilde{\theta})}$. The RHS can be expressed as

$$\rho q\Big\{\Big[\frac{2g_3}{g_2}\cos\theta - \cos(\theta - 2\tilde{\theta})\Big]\psi^0_x + \Big[\frac{2g_3}{g_2}\sin\theta + \sin(\theta - 2\tilde{\theta})\Big]\psi^0_y\Big\}. \tag{95}$$

This equation can now be used to solve for τ, by moving the terms on the RHS that are proportional to τ to the LHS, giving a RHS independent of τ, and noting that the unknown phase, θ_*, is independent of the amplitude, τ_*. We therefore first solve for θ_* by minimising

the mean absolute error between LHS and RHS for a range of θ_*. This is followed by a similar optimisation procedure for τ_*.

---

[1] IEA, *Offshore Wind Outlook 2019*, Tech. Rep. (International Energy Agency, 2019).

[2] IEA, *Renewable Energy Market Update 2023*, Tech. Rep. (International Energy Agency, 2023).

[3] D.-G. f. E. European Commission, *Offshore renewable energy strategy*, Tech. Rep. (Publications Office of the European Union, 2020).

[4] J. van Berkel, H. Burchard, A. Christensen, L. O. Mortensen, O. S. Petersen, and F. Thomsen, The effects of offshore wind farms on hydrodynamics and implications for fishes, Oceanogr. **33**, 108 (2020).

[5] R. Dorrell, C. Lloyd, B. Lincoln, T. Rippeth, J. Taylor, C. Caulfield, J. Sharples, J. Polton, B. Scannell, D. Greaves, R. Hall, and J. Simpson, Anthropogenic mixing in seasonally stratified shelf seas by offshore wind farm infrastructure, Front. Mar. Sci. **9**, 10.3389/fmars.2022.830927 (2022).

[6] T. Miles, S. Murphy, J. Kohut, S. Borsetti, and D. Munroe, Offshore wind energy and the Mid-Atlantic cold pool: a review of potential interactions, Mar. Technol. Soc. J. **55**, 72 (2021).

[7] K. Slavik, C. Lemmen, O. Kerimoglu, K. Klingbeil, and K. Wirtz, The large-scale impact of offshore wind farm structures on pelagic primary productivity in the southern North Sea, Hydrobiologia **845**, 35 (2019).

[8] U. Daewel, N. Akhtar, N. Christiansen, and C. Schrum, Offshore wind farms are projected to impact primary production and bottom water deoxygenation in the North Sea, Commun. Earth Environ. **3**, 10.1038/s43247-022-00625-0 (2022).

[9] National Academies of Sciences, Engineering, and Medicine, *Potential Hydrodynamic Impacts of Offshore Wind Energy on Nantucket Shoals Regional Ecology: An Evaluation from Wind to Whales* (The National Academies Press, Washington, DC, 2024).

[10] C. B. Hasager, P. Vincent, J. Badger, M. Badger, A. Di Bella, A. Peña, R. Husson, and P. J. H. Volker, Using satellite sar to characterize the wind flow around offshore wind farms, Energies **8**, 5413 (2015).

[11] A. Platis, S. Siedersleben, J. Bange, A. Lampert, K. Bärfuss, R. Hankers, B. Cañadillas, R. Foreman, J. Schulz-Stellenfleth, B. Djath, T. Neumann, and S. Emeis, First in situ evidence

of wakes in the far field behind offshore wind farms, Sci. Rep. **8**, 10.1038/s41598-018-20389-y (2018).

[12] N. Christiansen, U. Daewel, B. Djath, and C. Schrum, Emergence of large-scale hydrodynamic structures due to atmospheric offshore wind farm wakes, Front. Mar. Sci. **9**, 10.3389/fmars.2022.818501 (2022).

[13] H. Rennau, S. Schimmels, and H. Burchard, On the effect of structure-induced resistance and mixing on inflows into the Baltic Sea: A numerical study, Coastal Eng. **60**, 53 (2012).

[14] J. Carpenter, L. Merckelbach, U. Callies, S. Clark, L. Gaslikova, and B. Baschek, Potential impacts of offshore wind farms on North Sea stratification, PLoS ONE **11** (2016).

[15] L. Schultze, L. Merckelbach, J. Horstmann, S. Raasch, and J. Carpenter, Increased mixing and turbulence in the wake of offshore wind farm foundations, J. Geophys. Res. Oceans **125**, 10.1029/2019JC015858 (2020).

[16] K. Raghukumar, T. Nelson, M. Jacox, G. Chang, L. Cheung, and J. Roberts, Projected cross-shore changes in upwelling induced by offshore wind farm development along the California coast, Commun. Earth Environ. **4**, 10.1038/s41598-018-20389-y (2018).

[17] L. Schultze, L. Merckelbach, and J. Carpenter, Turbulence and mixing in a shallow shelf sea from underwater gliders, J. Geophys. Res. Oceans **122**, 10.1002/2017JC012872 (2017).

[18] J. Floeter, J. E. van Beusekom, D. Auch, U. Callies, J. Carpenter, T. Dudeck, S. Eberle, A. Eckhardt, D. Gloe, K. Hänselmann, M. Hufnagl, S. Janßen, H. Lenhart, K. O. Möller, R. P. North, T. Pohlmann, R. Riethmüller, S. Schulz, S. Spreizenbarth, A. Temming, B. Walter, O. Zielinski, and C. Möllmann, Pelagic effects of offshore wind farm foundations in the stratified North Sea, Prog. Oceanogr. **156**, 154 (2017).

[19] N. Christiansen, J. Carpenter, U. Daewel, N. Suzuki, and C. Schrum, The large-scale impact of anthropogenic mixing by offshore wind turbine foundations in the shallow North Sea, Front. Mar. Sci. **10** (2023).

[20] P. Cazenave, R. Torres, and J. Allen, Unstructured grid modelling of offshore wind farm impacts on seasonally stratified shelf seas, Prog. Oceanogr. **145**, 10.1016/j.pocean.2016.04.004 (2016).

[21] C. Garrett and P. Cummins, Maximum power from a turbine farm in shallow water, J. Fluid Mech. **714**, 634 (2013).

[22] N. Heaps, Linearized vertically-integrated equations for residual circulation in coastal seas,

682 Dtsch. Hydrogr. Z. **31**, 147 (1978).

683 [23] O. Strack, *Analytical Groundwater Mechanics* (Cambridge University Press, 2017).